THE JOURNAL OF PHYSICAL CHEMISTRY C

Article

pubs.acs.org/JPCC

Impact of Antisolvent Treatment on Carrier Density in Efficient Hole-Conductor-Free Perovskite-Based Solar Cells

Bat-El Cohen, Sigalit Aharon, Alex Dymshits, and Lioz Etgar*

Institute of Chemistry, Casali Center for Applied Chemistry, The Hebrew University of Jerusalem, Jerusalem 91904, Israel

Supporting Information

ABSTRACT: This work demonstrates antisolvent treatment of organo-metal halide perovskite film in hole-conductor-free perovskite-based solar cell, achieving impressive power conversion efficiency of 11.2% for hole-conductor-free cells with gold contact. We found that antisolvent (toluene) surface treatment affects the morphology of the perovskite layer, and importantly, it also affects the electronic properties of the perovskite. Conductive atomic force microscopy (cAFM) and surface photovoltage show that the perovskite film becomes more conductive after antisolvent treatment. Moreover, the antisolvent treatment suppresses the hysteresis commonly obtained for perovskite-based solar cells. When the perovskite alone is characterized, a $I-V$ plot of a single perovskite grain measured by cAFM shows that hysteresis vanishes after toluene treatment. During toluene treatment, excess halide and methylammonium ions are removed from the perovskite surface, leading to a net positive charge on the Pb atoms, resulting in a more conductive perovskite surface, which is beneficial for the hole-conductor-free solar cell structure. The reliability of the surface treatment was proved by calculating the statistical parameters Z score and p value, which were 2.5 and 0.012, respectively. According to these values, it can be concluded with 95% confidence that the average efficiency of cells fabricated via surface treatment is greater than the average efficiency of cells without surface treatment. The statistical data support the impact of surface treatment on the photovoltaic performance of perovskite solar cells.

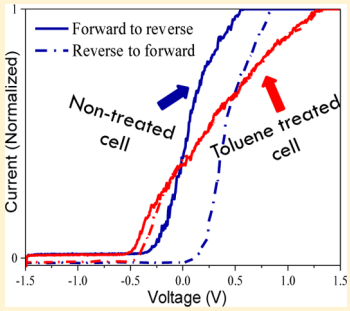

INTRODUCTION

Recently organic−inorganic perovskite has attracted a lot of attention due to its properties, which are suited to photovoltaic (PV) solar cells. The efficiency of perovskite-based solar cells has increased in a short time, achieving today 20.1% efficiency.[1] Perovskite-based solar cells can be used in several solar cell configurations, for example, mesoporous structure (similar to dye-sensitized solar cells) and planar structure (similar to thin-film cells).[2] Moreover, it was demonstrated that perovskite could function simultaneously as light harvester and hole conductor, simplifying the solar cell structure and potentially reducing its cost. A hole-conductor-free perovskite solar cell with gold contact currently achieves power conversion efficiency of 11.2%−11.4%, as discussed in this paper and elsewhere;[3] the power conversion efficiency for a hole-conductor-free perovskite solar cell with carbon electrode is 12.8%.[4] However, despite the tremendous increase in efficiency of perovskite-based solar cells, there are still several fundamental issues that must be investigated. One of the most discussed phenomena in the field of perovskite-based solar cells is the hysteresis effect. It has been demonstrated that hysteresis is present in perovskite solar cells and is heavily dependent on the solar cell structure as well as on the scan velocity during current voltage ($I-V$) measurements.[5] In the case of planar structure, the hysteresis is much more pronounced than in the mesoporous structure.[6,7] Moreover, fast and slow $I-V$ scan rates showed almost no hysteresis; however, in the case of the slow scan rate, quasi-steady-state conditions were achieved for accurate measurements.[8] The selective contacts are also an important factor in the hysteresis effect, where in the inverted architecture (such as ITO/PEDOT:PSS/perovskite/$PC_{61}BM$/Ca/Ag), small hysteresis is usually observed.[9] It has been reported that hysteresis is strongly dependent on pretreatment of the device by light biasing, which suggests that ion migration may be involved in the hysteresis effect.[4] In addition, it has been shown that the perovskite film could be passivated by surface treatments, resulting in better PV performance and in stable power conversion efficiency. Lewis bases were used to reduce the nonradiative recombination in the case of $CH_3NH_3PbI_{3-x}Cl_x$ perovskite, achieving approximately 16% efficiency for the planar architecture.[10] A mixture of γ-butyrolactone and dimethyl sulfoxide (DMSO) followed by toluene drop-casting showed smooth perovskite film forming a $CH_3NH_3I-PbI_2-$DMSO intermediate phase, achieving 16.2% efficiency without hysteresis.[11]

In this work, we demonstrate a high-efficiency hole-conductor-free perovskite solar cell with 11.2% power conversion efficiency (PCE) and small hysteresis. Antisolvent surface treatment was carried out, reducing the surface roughness of the perovskite film. The interface of the perovskite film with the metal contact is extremely important in the case of

Received: November 9, 2015
Revised: December 14, 2015

DOI: 10.1021/acs.jpcc.5b10994
J. Phys. Chem. C XXXX, XXX, XXX−XXX

the hole-conductor-free solar cell structure, due to the lack of hole conductor. It is important to note that we found the antisolvent treatment also affects the electronic properties of the perovskite film. Conductive atomic force microscopy (cAFM) and surface photovoltage (SPV) techniques were used to investigate more thoroughly the change in electronic properties of the perovskite following antisolvent treatment. The cAFM $I-V$ measurement was applied to a single perovskite crystal to gain information about the intrinsic properties of the perovskite itself, while surface photovoltage characterization revealed that perovskite became more intrinsic following antisolvent treatment.

EXPERIMENTAL SECTION

Device Fabrication. TiO_2 nanoparticles (20 nm, dyesol) were dispersed at 1:4 ratio in absolute ethanol and spin-coated (2000 rpm, 10 s) onto a substrate with the architecture SnO_2:F(FTO) conductive glass (15 $\Omega \cdot cm^{-1}$, Pilkington) coated by a layer of compact TiO_2 (TiDIP, 75% in 2-propanol, Aldrich). The substrate was then treated with $TiCl_4$.

$CH_3NH_3PbI_3$ was fabricated in two steps. First, PbI_2 (Aldrich, 99%, 1 M in dimethylformamide) was dropped onto the substrate. After 3 min, the substrate was spun at 2000 rpm for 25 s and then annealed for 30 min at 70 °C. Next, the substrate was dipped into CH_3NH_3I [methylammonium iodide (MAI), synthesized as described earlier][13] solution (0.06 M in 2-propanol) for 30 s, and then annealed at 90 °C for 30 min, forming the dark perovskite layer.

For the toluene treatment, substrates were dipped into MAI solution after the annealing of the PbI_2, and then directly spun at 4000 rpm for 30 s. 45 μL of toluene were dropped on the substrate during spin. The substrate was then annealed at 90 °C for 30 min. Gold (40 nm) was deposited by thermal evaporation at 10^{-6} Torr as contacts.

Atomic Force Microscopy. Scanning probe microscope measurements were made by using Dimension 3100 Nanoscope V in conductive tunneling atomic force microscopy (TUNA) mode. The $I-V$ single-grain measurement was performed with an atomic force microscopy (AFM) conductive tip (SCM-PIT). A voltage scan was applied to the cell from −1.5 to 1.5 V at a scan rate of 0.5 Hz. The measurement was carried out in the dark with a 670 nm laser beam.

High-Resolution Scanning Electron Microscopy. The images were obtained on a Sirion high-resolution scanning electron microscope (HR-SEM) from FEI (Field Emission Instruments, Eindhoven, The Netherlands). The measurement conditions were 5 kV at various magnifications, as seen on the data bar of the images.

Photovoltaic Characterization. Photovoltaic measurements were made on a New Port system, composed of an Oriel $I-V$ test station with an Oriel Sol3A simulator. The solar simulator is class AAA for spectral performance, uniformity of irradiance, and temporal stability. The solar simulator is equipped with a 450 W xenon lamp. The output power is adjusted to match AM1.5 global sunlight (100 $mW \cdot cm^2$). The spectral match classifications are IEC60904-9 2007, JIC C 8912, and ASTM E927-05. $I-V$ curves were obtained by applying an external bias to the cell and measuring the generated photocurrent with a Keithley model 2400 digital source meter. Voltage step was 10 mV and delay time of photocurrent was 40 ms.

Incident Photon-to-Electric Current Conversion Efficiency. An Oriel IQE-200 instrument was used to determine the monochromatic incident photon-to-electric current conversion efficiency (IPCE). Under full computer control, light from a 150 W xenon arc lamp was focused through a monochromator in the 300−1800 nm wavelength range onto the photovoltaic cell under test. The monochromator was incremented through the visible spectrum to generate the IPCE (λ) as defined by IPCE (λ) = 12 400($J_{sc}/\lambda\phi$), where λ is wavelength, J_{sc} is short-circuit photocurrent density (milliamperes per square centimeter), and ϕ is incident radiative flux (milliwatts per square centimeter). Photovoltaic performance was measured by using a metal mask with an aperture area of 0.04 cm^2.

Surface Photovoltage Spectroscopy. Surface photovoltage spectroscopy (SPS) was performed on the SKP5050-SPS040 system. Contact potential difference (CPD) between the sample and the vibrating tip was measured by the Kelvin probe technique. Samples were measured in a Faraday cage under air environment. For SPS measurements, the samples were illuminated with a 150 W quartz tungsten halogen lamp. The wavelength resolution was 2 nm. Before the measurement, samples were stabilized with a tip for about 1 h. The scan direction was from long to short wavelength. The work function (WF) was calculated according to $WF_{sample} = WF_{tip} - CPD$ (tip − sample). The work function of the tip was calibrated above the gold stage.

X-ray Diffraction. X-ray diffraction (XRD) measurements were performed on the D8 Advance diffractometer (Bruker AXS, Karlsruhe, Germany) with a secondary graphite monochromator, 2° Soller slits, and a 0.2 mm receiving slit. XRD patterns within the range 3−75° 2θ were recorded at room temperature by use of Cu Ka radiation (λ = 1.5418 Å) under the following measurement conditions: tube voltage of 40 kV, tube current of 40 mA, step-scan mode with a step size of 0.02° 2θ, and counting time of 1 s/step.

Transmittance and Reflection Measurements. These measurements were performed on a Jasco V-670 spectrophotometer, between 300 and 850 nm wavelengths.

RESULTS AND DISCUSSION

In this work we describe high-efficiency hole-transport-material (HTM) -free perovskite-based solar cells treated with antisolvent of the perovskite film, improving the film roughness and enhancing its conductivity.

Figure 1A presents a schematic illustration of the $CH_3NH_3PbI_3$ deposition process. The perovskite deposition process is based on the two-step deposition method described earlier[12,13] with the addition of antisolvent (toluene) treatment on the perovskite film. We observed enhanced photovoltaic performance as a result of toluene treatment, discussed below. Figure 1B shows the XRD spectra of perovskite film without toluene treatment (standard, black) and with toluene treatment (red). No observable variations were recognized in the XRD spectra, which suggests that no crystallographic changes occurred. A schematic illustration of the HTM-free solar cell structure is presented in Figure 1C. The solar cell structure consists of fluorine tin oxide (FTO) glass/dense TiO_2/TiO_2 mesoporous/perovskite film/Au, as previously reported by us.[14]

Toluene treatment of the perovskite film was previously reported to increase the photovoltaic performance of perovskite-based solar cells with hole transport material.[10] In this work, since no hole transport material is being used, the interface of perovskite with the metal contact is significantly important and can play an important role in the photovoltaic

DOI: 10.1021/acs.jpcc.5b10994
J. Phys. Chem. C XXXX, XXX, XXX−XXX

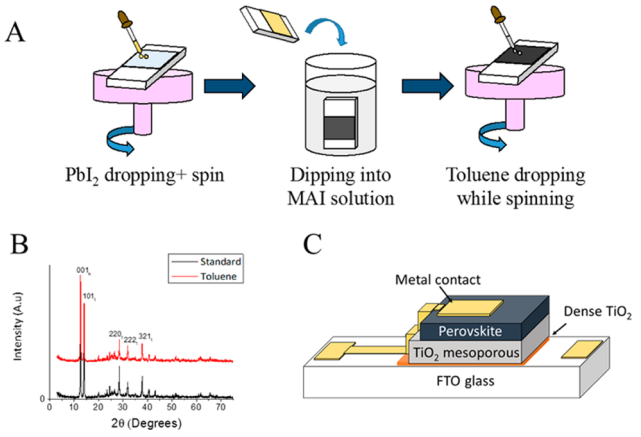

Figure 1. (A) Schematic presentation of antisolvent treatment for perovskite film deposition. (B) XRD spectra of standard and toluene-treated perovskite films. (C) Structure of HTM-free perovskite-based solar cell. MAI = CH_3NH_3I.

performance of these HTM-free cells. The current−voltage (I−V) curve of the HTM-free perovskite-based solar cell is presented in Figure 2A with open-circuit voltage (V_{oc}) of 0.91 V, fill factor (FF) of 0.65, and current density (J_{sc}) of 19 mA/cm^2, corresponding to power conversion efficiency of 11.2%. The normalized external quantum efficiency (EQE) curve is presented in the inset of Figure 2A. Integration over the EQE spectrum gives current density of 16.2 mA/cm^2, in good agreement with J_{sc} obtained from the solar simulator. Figure 2B presents statistics for standard cells and for cells with toluene treatment. It is noted that the average power conversion efficiency of the standard cells is 8% ± 1%, while that of the toluene-treated cells is 9% ± 1%. It is clear that toluene treatment improves the photovoltaic performance of HTM-free cells. J_{sc} and FF change slightly, while V_{oc} is the parameter most affected by this treatment. V_{oc} is larger by 0.05 V on average in the case of toluene-treated cells. This enhancement can be related to the improved morphology and conductivity as discussed below. Table S1 presents the improvement in PV parameters as a result of toluene treatment. In order to prove the reliability of the results, statistical analysis was performed as described by Luber and Buriak.[15] First the Z score is determined according to $Z = (x_1 - x_2)/(\sigma/\sqrt{N})$, where x_2 is the average PCE of nontreated cells, x_1 is the average PCE of treated cells, σ is the standard deviation of treated cells, and N is the number of cells. From these parameters the Z score was equal to 2.5, which correspond to a p-value of 0.012. Since the p-value is lower than 0.05, it can be concluded with 95% confidence that the average PCE of cells fabricated with toluene treatment is greater than the average PCE of cells without toluene treatment. This further supports the statistical significance of the results.

To investigate the morphology and electronic effects of toluene treatment on the perovskite film, we performed scanning electron microscopy (SEM), normal and conductive atomic force microscopy (AFM and cAFM) and surface photovoltage measurements. Top-view SEM images are presented in Figure 3A,D for toluene-treated and nontreated samples, respectively. Red circles indicate the pinholes observed in the perovskite film. It can be seen that for perovskite film after toluene treatment, there are fewer pinholes than in the perovskite film made by two-step deposition without additional treatment. It can be concluded that the perovskite coverage improved as a result of toluene treatment. (Additional top-view SEM images of treated and untreated films can be found in Figure S1.) In addition, AFM was performed to observe the root-mean-square (rms) roughness of the perovskite film surface. The rms roughness for toluene-treated film is 30 nm, while for standard (nontreated) film, the rms roughness is 40 nm, indicating that in addition to the better coverage achieved by toluene treatment, the surface roughness is also smoother when treated with toluene. Since the perovskite film has a direct attachment to the metal contact in the HTM-free configuration, better coverage and lower rms roughness of the toluene-treated cells contribute to better photovoltaic performance. Figure 3B,E shows AFM morphology and corresponding cAFM measurements (current mapping) of toluene-treated and nontreated $CH_3NH_3PbI_3$ perovskite films. Conductivity of the perovskite film treated with toluene is larger (by 10 times over the conductive grains) than that of nontreated perovskite film (Figure 3, panel C versus panel F). No bias was applied during the conductivity measurements. In the toluene-treated film most of the grains are conductive (Figure 3C), while in the nontreated perovskite film the average conductivity is much lower, with slightly higher conductivity at the grain boundaries (Figure 3F).

Figure 4A,B shows the current−voltage (I−V) plots of a single conductive grain, in forward and reverse scans of nontreated and toluene-treated perovskite films, respectively. The insets of these panels present I−V plots of a single

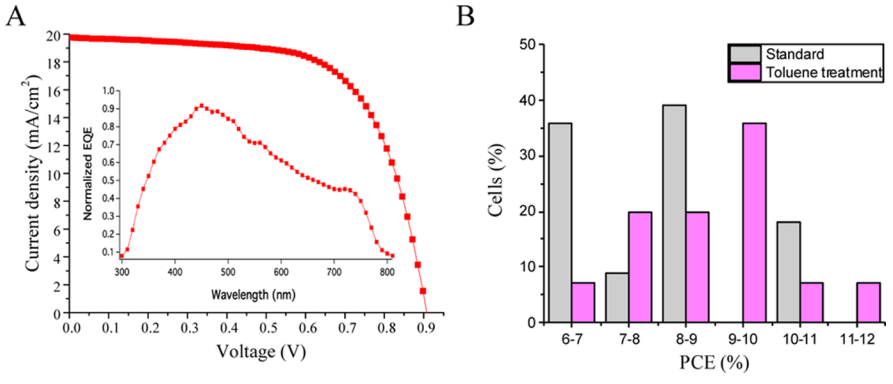

Figure 2. (A) I−V curve of toluene-treated HTM-free perovskite-based solar cell. (Inset) EQE curve of the corresponding cell. (B) Statistics of the efficiency of cells without and with toluene treatment. Statistical analysis was performed for a total number of 28 electrodes, which is equivalent to 84 cells.

DOI: 10.1021/acs.jpcc.5b10994
J. Phys. Chem. C XXXX, XXX, XXX−XXX

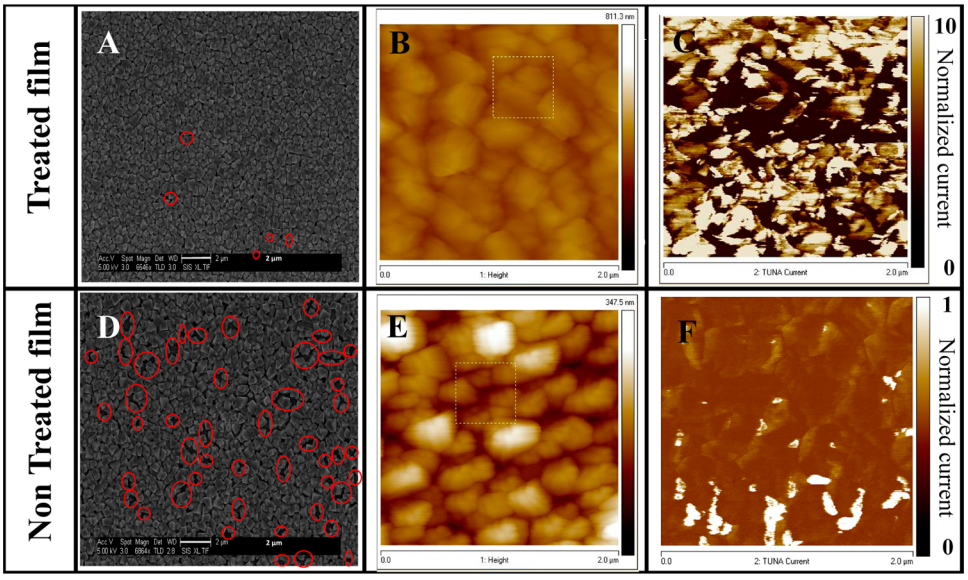

Figure 3. (A, D) SEM figures of (A) toluene-treated and (D) standard solar cells. Red circles indicate pinholes in the perovskite film. (B, E) Morphology AFM images of (B) toluene-treated and (E) standard solar cells. The rms roughness for standard cell is 40 nm and for toluene-treated cell is 30 nm. Current mapping was measured by cAFM without bias. (C, F) Conductivity of (C) toluene-treated and (F) nontreated (standard) perovskite films.

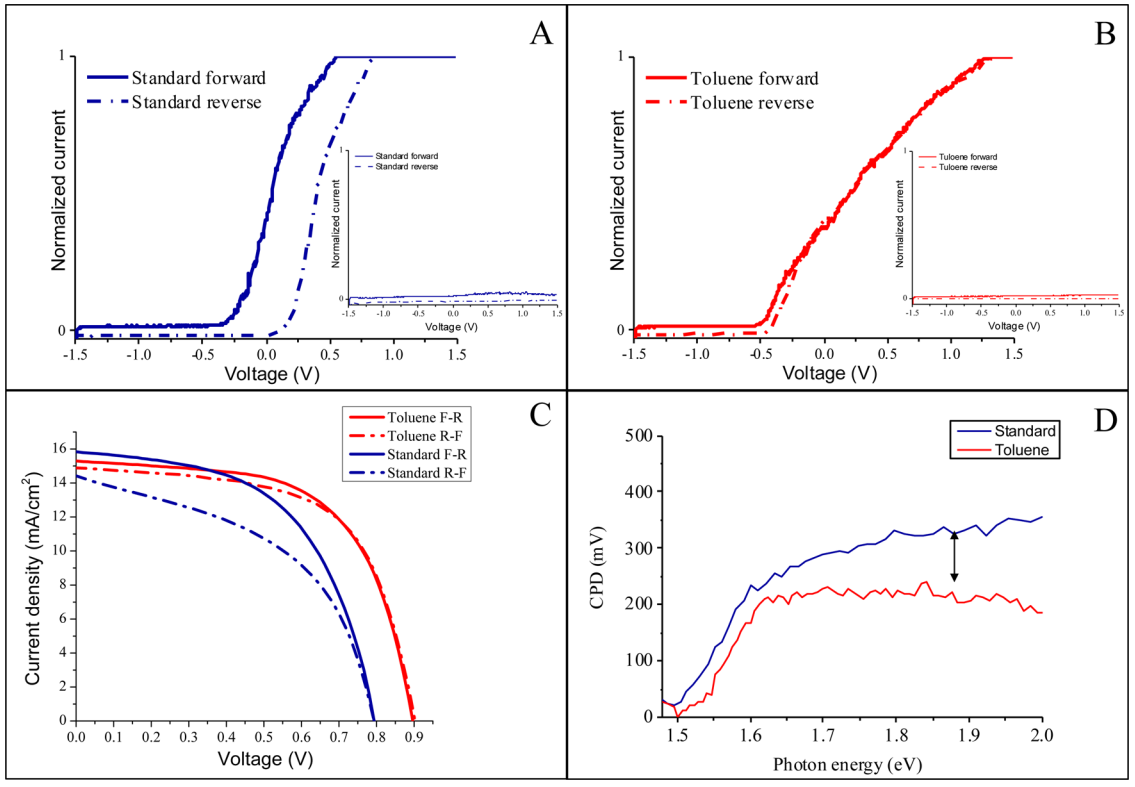

Figure 4. *I*–*V* plots measured on a single perovskite grain by cAFM (A) without and (B) with toluene treatment. Inset: IV plot of single nonconductive grain. (C) Current–voltage curves measured by solar simulator for HTM-free perovskite solar cell. The scan rate was 0.087 V/s. (D) Surface photovoltage measurements of toluene-treated and nontreated perovskite films. Black arrow indicates the difference in CPD. F = forward, R = reverse.

nonconductive grain, forward and reverse scans for the two different treatments.

Several conclusions can be extracted from this measurement. (i) No hysteresis observed in the toluene-treated film compared to film without toluene treatment. Clearly, the toluene treatment suppresses hysteresis. (ii) In the case of nontreated film (Figure 4A), the cAFM measurements show direct experimental observation of the memory properties of the perovskite.[17] (iii) Looking at the *I*–*V* slope in the linear region for both films (Figure 4A,B), it can be observed that the slope in the *I*–*V* plot is smaller for treated perovskite than for nontreated perovskite. The difference in the slope suggests

DOI: 10.1021/acs.jpcc.5b10994
J. Phys. Chem. C XXXX, XXX, XXX–XXX

different carrier densities of the two samples.[16] It appears that, after toluene treatment, the sample becomes more intrinsic (intrinsic semiconductor means a pure semiconductor without any significant dopant species present) than without toluene treatment. (iv) In the case of nonconductive grains, the $I-V$ plots were almost zero (insets of Figure 4A,B). From the cAFM measurements, it seems that the toluene treatment does not just passivate the perovskite film but also changes its electronic properties.

Figure 4C shows current−voltage curves, forward and reverse scans, measured by solar simulator under 1-sun illumination of HTM-free cells, treated with toluene and nontreated. The difference between treated and nontreated cells is observable. Hysteresis in the nontreated cells is much more pronounced than in the toluene-treated cells, where a small change appears between the forward-to-reverse scan and the reverse-to-forward scan. However, in contrast to the $I-V$ plot of toluene-treated film measured by cAFM, where no hysteresis was observed (Figure 4B), in the current−voltage measurements of the complete solar cell (Figure 4C) there is still a small shift between the two scan directions. This important result suggests that the origin of hysteresis has more than one influence, when clearly one influence on hysteresis is related to the intrinsic properties of the perovskite, probably the memory effect.[16]

To further elucidate the influence of toluene treatment on the electronic properties of perovskite, the surface photovoltage technique was applied on toluene-treated and nontreated perovskite films (Figure 4D). The main observation noted from surface photovoltage spectra is the difference in contact potential difference (ΔCPD). The contact potential difference is higher by ≈100 mV (marked with an arrow in Figure 4D) for standard perovskite film (nontreated film) compared to the toluene-treated film. The difference in contact potential difference suggests that the quasi-Fermi level of toluene-treated film is higher (less negative by 0.1 eV) than the quasi-Fermi level of nontreated toluene film. Therefore, it can be concluded that, subsequent to toluene treatment, the perovskite film becomes slightly more intrinsic, as also observed by the cAFM measurements. In addition, the surface photovoltage approximately indicates the band gap of the material. The band gap of toluene-treated film extracted from the surface photovoltage spectra is 1.57 eV, while for nontreated film the band gap is 1.56 eV, which suggests that there is no observable change in the band gap.

Scheme 1 illustrates the effect of toluene treatment on the perovskite surface. We suggest that, during toluene treatment, excess halide and methylammonium ions are removed from the surface by forming a complex with the solvent, similar to the previous report by Seok and co-workers.[11] This creates a net positive charge on the Pb atoms. Snaith et al.[10] have reported on a similar effect before the application of Lewis base passivation.

This interpretation is correlated to the results obtained from cAFM. The cAFM measurement indicates that the surface after toluene treatment is more conductive than before toluene treatment, which agrees well with the net positive charge on Pb atoms in the case of treated perovskite surface. In addition, the net positive charge of the perovskite surface after toluene treatment is beneficial for PV performance. Net positive charge of the perovskite surface could accept electrons more efficiently, which is useful for the interface of perovskite with gold.

Scheme 1. Effect of Toluene Treatment on the Perovskite Surface[a]

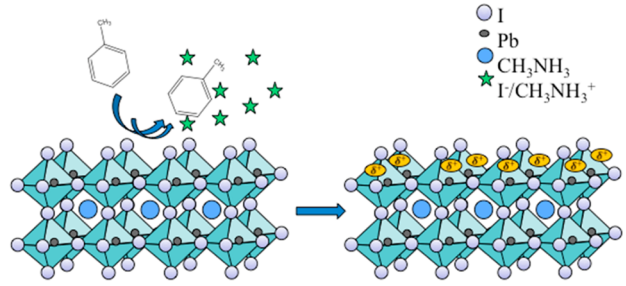

[a]During toluene treatment, excess halide and methylammonium ions are removed from the surface, which creates a net positive charge on the Pb atoms.

CONCLUSIONS

This work presents the impact of a simple antisolvent (toluene) treatment on the photovoltaic performance of hole-transport-material-free perovskite solar cell, exceeding 11% efficiency. The antisolvent treatment changes the film morphology and improves the film coverage, which is beneficial for the performance of these HTM-free cells. Conductive atomic force microscopy and surface photovoltage techniques show that the electronic properties of the perovskite film also change due to antisolvent treatment: the perovskite film became slightly more intrinsic, further contributing to the enhanced performance. During toluene treatment, halide and methylammonium ions are removed from the surface, which creates a net positive charge on the Pb atoms, resulting in more conductive surface of the perovksite, which is beneficial for the HTM-free solar cell structure.

Importantly, cAFM measurements on a single perovskite grain confirmed the suppression of hysteresis due to antisolvent treatment, and this helps us to understand the origin of hysteresis in perovskite-based solar cells. Elucidating the effect of antisolvent treatment on perovskite properties (electronic and morphology) is important and beneficial. The knowledge gained is not only limited to perovskite-based solar cells but also applies to light-emitting diodes and lasing applications, which have recently involved the promising organo-metal perovskite material.

ASSOCIATED CONTENT

Supporting Information

The Supporting Information is available free of charge on the ACS Publications website at DOI: 10.1021/acs.jpcc.5b10994.

One table listing PV parameters for treated and standard cells and one figure with additional SEM images of the perovskite surface for toluene-treated and standard cells (PDF)

AUTHOR INFORMATION

Corresponding Author

*E-mail lioz.etgar@mail.huji.ac.il.

Notes

The authors declare no competing financial interest.

ACKNOWLEDGMENTS

We acknowledge the financial support of Israel Alternative Energy Foundation (I-SAEF), the Ministry of Industry Trade

DOI: 10.1021/acs.jpcc.5b10994
J. Phys. Chem. C XXXX, XXX, XXX−XXX

and Labor Office of the Chief Scientist, Kamin Project 50303, the Tashtiot Project of the Office of the Chief Scientist, and the German Israel Foundation for Young Researchers.

REFERENCES

(1) http://www.nrel.gov/ncpv/images/efficiency_chart.jpg.
(2) Gamliel, S.; Etgar, L. Organo-metal perovskite based solar cells: sensitized versus planar architecture. *RSC Adv.* **2014**, *4*, 29012−29021.
(3) Shi, J.; Wei, H.; Lv, S.; Xu, X.; Wu, H.; Luo, Y.; Li, D.; Meng, Q. Control of Charge Transport in the Perovskite $CH_3NH_3PbI_3$ Thin Film. *ChemPhysChem* **2015**, *16*, 842−847.
(4) Mei, A.; Li, X.; Liu, L.; Ku, Z.; Liu, T.; Rong, Y.; Xu, M.; Hu, M.; Chen, J.; Yang, Y.; Grätzel, M.; Han, H. A hole-conductor−free, fully printable mesoscopic perovskite solar cell with high stability. *Science* **2014**, *345*, 295−298.
(5) Snaith, H. J.; Abate, A.; Ball, J. M.; Eperon, J. E.; Leijtens, T.; Noel, K. N.; Stranks, D. S.; Wang, J. T.-W.; Wojciechowski, K.; Zhang, W. Anomalous Hysteresis in Perovskite Solar Cells. *J. Phys. Chem. Lett.* **2014**, *5*, 1511−1515.
(6) Dualeh, A.; Moehl, T.; Tétreault, N.; Teuscher, J.; Gao, P.; Nazeeruddin, K. M.; Grätzel, M. Impedance Spectroscopic Analysis of Lead Iodide Perovskite-Sensitized Solid-State Solar Cells. *ACS Nano* **2014**, *8*, 362−373.
(7) Sanchez, S. R.; Gonzalez-Pedro, V.; Lee, J.-W.; Park, N.-G.; Kang, Y. S.; Mora-Sero, I.; Bisquert, J. Slow Dynamic Processes in Lead Halide Perovskite Solar Cells. Characteristic Times and Hysteresis. *J. Phys. Chem. Lett.* **2014**, *5* (13), 2357−2363.
(8) Unger, E. L.; Hoke, E. T.; Bailie, C. D.; Nguyen, W. H.; Bowring, A. R.; Heumüller, T.; Christoforo, M. G.; McGehee, M. D. Hysteresis and transient behavior in current−voltage measurements of hybrid-perovskite absorber solar cells. *Energy Environ. Sci.* **2014**, *7*, 3690−3698.
(9) Tripathi, N.; Yanagida, M.; Shirai, Y.; Masuda, T.; Han, L.; Miyano, K. Hysteresis-free and highly stable perovskite solar cells produced *via* a chlorine-mediated interdiffusion method. *J. Mater. Chem. A* **2015**, *3*, 12081−12088.
(10) Noel, K. N.; Abate, A.; Stranks, D. S.; Parrott, S. E.; Burlakov, M. V.; Goriely, A.; Snaith, H. J. Enhanced Photoluminescence and Solar Cell Performance *via* Lewis Base Passivation of Organic−Inorganic Lead Halide Perovskites. *ACS Nano* **2014**, *8* (10), 9815−9821.
(11) Jeon, N. J.; Noh, H. J.; Kim, C. Y.; Yang, S. W.; Ryu, S.; Seok, S. Solvent engineering for high-performance inorganic-organic hybrid perovskite solar cells. *Nat. Mater.* **2014**, *13*, 897−903.
(12) Cohen, B. E.; Gamliel, S.; Etgar, L. Parameters influencing the deposition of methylammonium lead halide iodide in hole conductor free perovskite-based solar cells. *APL Mater.* **2014**, *2*, No. 081502.
(13) Burschka, J.; Pellet, N.; Moon, S.-J.; Humphry-Baker, R.; Gao, P.; Nazeeruddin, M. K.; Grätzel, M. Sequential deposition as a route to high-performance perovskite-sensitized solar cells. *Nature* **2013**, *499*, 316−319.
(14) Aharon, S.; Gamliel, S.; Cohen, B.-E.; Etgar, L. Depletion region effect of highly efficient hole conductor free $CH_3NH_3PbI_3$ perovskite solar cells. *Phys. Chem. Chem. Phys.* **2014**, *16*, 10512−10518.
(15) Luber, J. E.; Buriak, M. J. Reporting Performance in Organic Photovoltaic Devices. *ACS Nano* **2013**, *7*, 4708−4714.
(16) Strukov, D. B.; Snider, G. S.; Stewart, D. R.; Williams, S. The missing memristor found. *Nature* **2008**, *453*, 80−83.
(17) Ahmad, M.; Zhao, J.; Iqbal, J.; Miao, W.; Xie, L.; Mo, R.; Zhu, J.; Mashkoor, A.; et al. Conductivity enhancement by slight indium doping in ZnO nanowires for optoelectronic applications. *J. Phys. D: Appl. Phys.* **2009**, *42*, No. 165406.

DOI: 10.1021/acs.jpcc.5b10994
J. Phys. Chem. C XXXX, XXX, XXX−XXX